JOURNAL OF GEOPHYSICAL RESEARCH, VOL. 97, NO. C8, PAGES 12,607–12,618, AUGUST 15, 1992

A Description of Water Types on the Mackenzie Shelf of the Beaufort Sea During Winter

R. M. MOORE

Department of Oceanography, Dalhousie University, Halifax, Nova Scotia, Canada

H. MELLING

Institute of Ocean Sciences, Sidney, British Columbia, Canada

K. R. THOMPSON

Department of Oceanography, Dalhousie University, Halifax, Nova Scotia, Canada

For a number of years during the 1980s, observations of the physical and chemical properties of seawater in the southeastern Beaufort Sea have been acquired in late winter. The most complete data set, from 1987, has been used in a comparison of winter and summer [Macdonald et al., 1989] water properties in the area. Most obvious is an increase in the salinity of surface waters in winter. The magnitude of this increase varies dramatically from year to year. Part of the increase is a consequence of brine rejection during the growth of sea ice, and part is associated with an intrusion over the shelf of a water mass of high nutrient and low oxygen concentrations which is a feature of the entire western Arctic Ocean. Principal component analysis was used to allow all five chemical tracers to be combined and viewed simultaneously. The properties of the upper 120 m are found to lie, to a close approximation, on a plane. This leads us to a simple interpretation based on a three-component mixing model involving river runoff, water from the nutrient maximum, and an offshore near-surface component. It is shown that the best fit plane occupied by arctic surface waters in the Beaufort Sea closely matches that defined by the influences of river inflow, of the freeze-melt cycle, and of photosynthesis and respiration. However, the effects of freezing/melting and of river inflow cannot be clearly distinguished using the chosen suite of tracers. It has been determined that if the waters of the upper 250 m are to be represented in the same manner, a fourth end member is required.

INTRODUCTION

From observations made during the late summer of 1986, *Carmack et al.* [1989] and *Macdonald et al.* [1989] have described the summertime distribution of water masses over the Mackenzie shelf of the Beaufort Sea. There is a marked contrast between the water properties that they describe and those which have been observed in the wintertime over a number of years. These differences are mainly due to the much reduced supply of fresh water to the system from the Mackenzie River in wintertime, and to the influence of salt addition from the growth of sea ice. Both these factors will apply during any winter season, though in varying degree. Other factors can also be important, in particular the efficiency with which low-salinity water is exported from the shelf during the late summer and autumn and the extent to which salt is supplied to the surface layer from below by the processes of upwelling and entrainment. Other differences between the waters in summer and winter involve the concentration of nutrients (nitrate, silicate, and phosphate). This paper uses data collected during the late winters of 1985–1987 as a basis for the description of the winter water masses.

The collection of the data described here was motivated by interest in the production of dense waters over the continental shelves of the Arctic Ocean by freezing during the winter. Of the total area of this ocean (1.3×107 km^2), approximately 35% is continental shelf where water depth is less than 200 m. Recognition of the potential importance of freezing for dense water formation goes back to *Nansen* [1906], though evidence for its actual effect on waters in the Arctic basins has been rather limited, especially for the Canada Basin. *Midttun* [1985] has provided evidence that the process occurs in the Barents Sea where, he reports, it is a fairly regular event on the Novaya Zemlya shelf. *Aagaard et al.* [1981] discussed the possible locations in which the process may be important and provided evidence for its occurrence in the shallow waters of the Chukchi Sea; further data from the same area are reported by *Aagaard et al.* [1985*a*]. *Melling and Lewis* [1982] have discussed the production of cold subsurface arctic waters from salinization occurring on the continental shelves and have provided evidence from the Beaufort Sea. *Aagaard* [1989] argues that these shelf processes influence the waters exported from the Arctic Ocean through western Fram Strait, which mix with deep water from the Greenland Sea to give Norwegian Sea deep waters; thence the influence is transferred to the dense flows into the North Atlantic.

We wish to determine whether the chemical properties of winter shelf waters which may ultimately ventilate the arctic halocline are modified by their period of residence on the continental shelf. The Mackenzie shelf of the Beaufort Sea is a covenient laboratory for this investigation of wintertime oceanographic phenomena which may occur widely in arctic shelf seas.

Field studies carried out in the years 1985–1987 did not show the presence on the Mackenzie shelf of waters having salinities (and therefore densities) sufficiently high to ventilate the halocline. Since the seawater properties observed during these three winters were similar and lay between the extremes which have been observed in this area [e.g., *Melling* 1992], it is reasonable to consider them as

Paper number 92JC00842.
0148-0227/92/92JC-00842 $05.00

median conditions in the Beaufort Sea, at least for the 1980s. These properties are compared with those in summertime, described by *Macdonald et al.* [1989]. Our most complete data sets are for the years 1986 and 1987; the second of these will be the focus of this paper. Very high surface salinities were observed over the entire area in 1981, but no sampling for chemical constituents was carried out at that time, and the type of analysis presented in this paper could not be attempted. The 1981 observations are discussed by *Melling* [1992].

In the following description of the water properties, information on the nature of the interacting water types could have been derived directly from examination of plots of individual properties, one against another. However, on account of the number of chemical properties for which we have data, we have used principal component analysis to combine and view all the tracers simultaneously. If this procedure shows that all the tracers lie within a plane, as in our case, it may be possible to identify three mixing end-members.

A tentative assumption made in this work is that the nutrient concentrations could be treated as water mass tracers, since during the wintertime they would not be affected by biological uptake. It was recognized that regeneration processes might be providing a source of additional nutrients to the system [*Jones and Anderson*, 1986] and at the same time causing a possible reduction in the dissolved oxygen concentrations. In the treatment used, such processes should be manifest as nonlinearities in the mixing of properties, or equivalently, in the existence of additional end-members.

METHODS

The study area is shown in Figure 1 with the location of sampling sites in 1987. Each year's survey was done in late March or early April, and sampling was completed in about 1 week. At each location water samples were collected through the ice using syringe type samplers deployed at depths from the surface to 250 m with a spacing between samples of 5–20 m. Water samples were immediately drawn off in a warmed environment with subsamples being taken for the determination of salinity, nutrients (silicate, phosphate, and nitrate), and dissolved oxygen. Samples were analyzed usually within 24 hours. All nutrients were measured by standard procedures described by *Strickland and Parsons* [1972]. The error in silicate measurements is calculated as $\pm 0.3\ \mu M$ (i.e. $\pm 2\sigma$), and the nitrate error is $\pm 0.2\ \mu M$. The phosphate error, calculated as $\pm 0.07\ \mu M$, is higher than the method would normally give because the analyses had to be done with a short path-length (2 cm) cell. Dissolved oxygen was measured by an automated Winkler procedure on 125-mL samples. While repeated titration of aliquots of the same iodine sample gave a precision of $\pm 0.8\ \mu M$ (i.e., $\pm 2\sigma$), a more realistic estimate of precision for the entire procedure including sampling and preservation is $\pm 2\ \mu M$.

Detailed profiles of sea water temperature and salinity were acquired using a Guildline 8706 conductivity-temperature-depth probe (CTD) sampling at 25 Hz, and descending at a controlled rate of 1.6 m/s. Useable data were obtained between about 0.5 m beneath the lower surface of the ice, and about 2 m above the seafloor. The probe was equipped with a seafloor proximity switch to permit such close approach without hazard. For temperature, in situ checks against precision thermistors prior to each profile provided the offset for the linear calibration equation, while laboratory data over a wider temperature range provided the slope. Temperatures are judged to be accurate to 0.003°C.

For pressure, a laboratory dead-weight tester provided the overall shape of the calibration curve, at a temperature close to that of field use (0°C). An offset was calculated for each profile by lowering the probe to a known depth

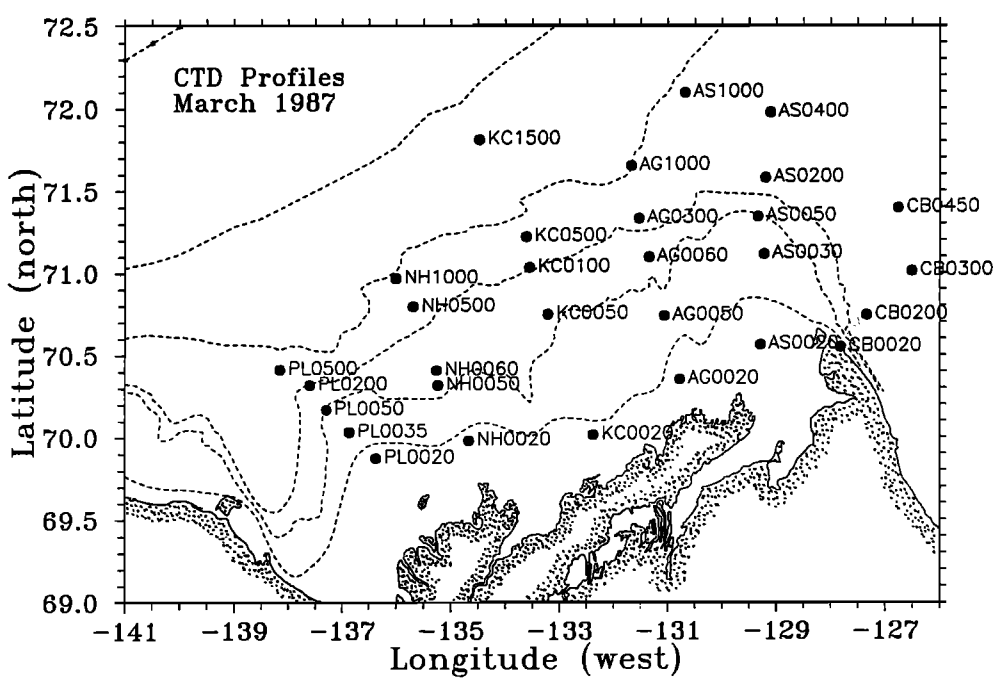

Fig. 1. A map of the southeastern Beaufort Sea showing the location of seawater sampling in 1987. The isobaths are 25, 50, 200, 1000, 2000 and 3000 m.

and noting the difference between the indicated pressure and that calculated. Pressure values are considered accurate to 0.3 dbar and precise to 0.1 dbar.

A single water sample was collected in conjunction with each profile for calibration of the conductivity cell. This sample was taken at a depth of minimal gradient in salinity, with the probe in motion during the downward cast. A microswitch attached to the bottle signalled the exact moment of sample acquisition on the CTD record. These samples were analyzed in triplicate using a Guildline Autosal salinometer. The overall accuracy of the calibrated salinity profiles is estimated to be in the range 0.005 to 0.008. Under difficult arctic conditions, careful procedures are required to achieve the quoted accuracies.

In addition to collection of temperature-salinity (T-S) data by CTD, the water samples collected for chemical measurements were also analysed for salinity using a Guildline Autosal salinometer. The accuracy of the salinity of these samples is estimated as ± 0.01.

RESULTS AND DATA ANALYSIS

All of the tracer measurements acquired in 1987 are shown as scatter plots in Figure 2. Later in this paper we demonstrate how these measurements can be condensed into a more manageable form through the application of principal component analysis. The same data are presented in Figure 3 as vertical sections running across the shelf. The three westerly observation lines (near the mouths of the Mackenzie River) have been grouped together (denoted sections 1–3), and the two easterly lines have been grouped as sections 4 and 5. A section is not included for the phosphate concentration due to its close similarity to that for silicate.

In wintertime, the uppermost 20–40 m over the continental shelf is occupied by a well-mixed layer of salinity lower than that in the halocline of the arctic basin but higher than that found at the surface in the basin in summer. This is in contrast to the situation in summertime [*Carmack et al.*, 1989] when the surface layer is much shallower (~5–10 m) and of much lower salinity (~ 20). *Carmack et al.* [1989] note a sharp rise to salinities typical of the wintertime surface layer at about 20 m depth in late summer. Beneath the wintertime surface layer the salinity rises steeply, as is illustrated by the sections in Figure 3.

A wintertime surface layer of intermediate salinity is characteristic of arctic waters in general and reflects the combined effects of significant river inflow to the Arctic Ocean and of the growth-melt cycle of sea ice. However, in the southeastern Beaufort Sea, these effects are amplified

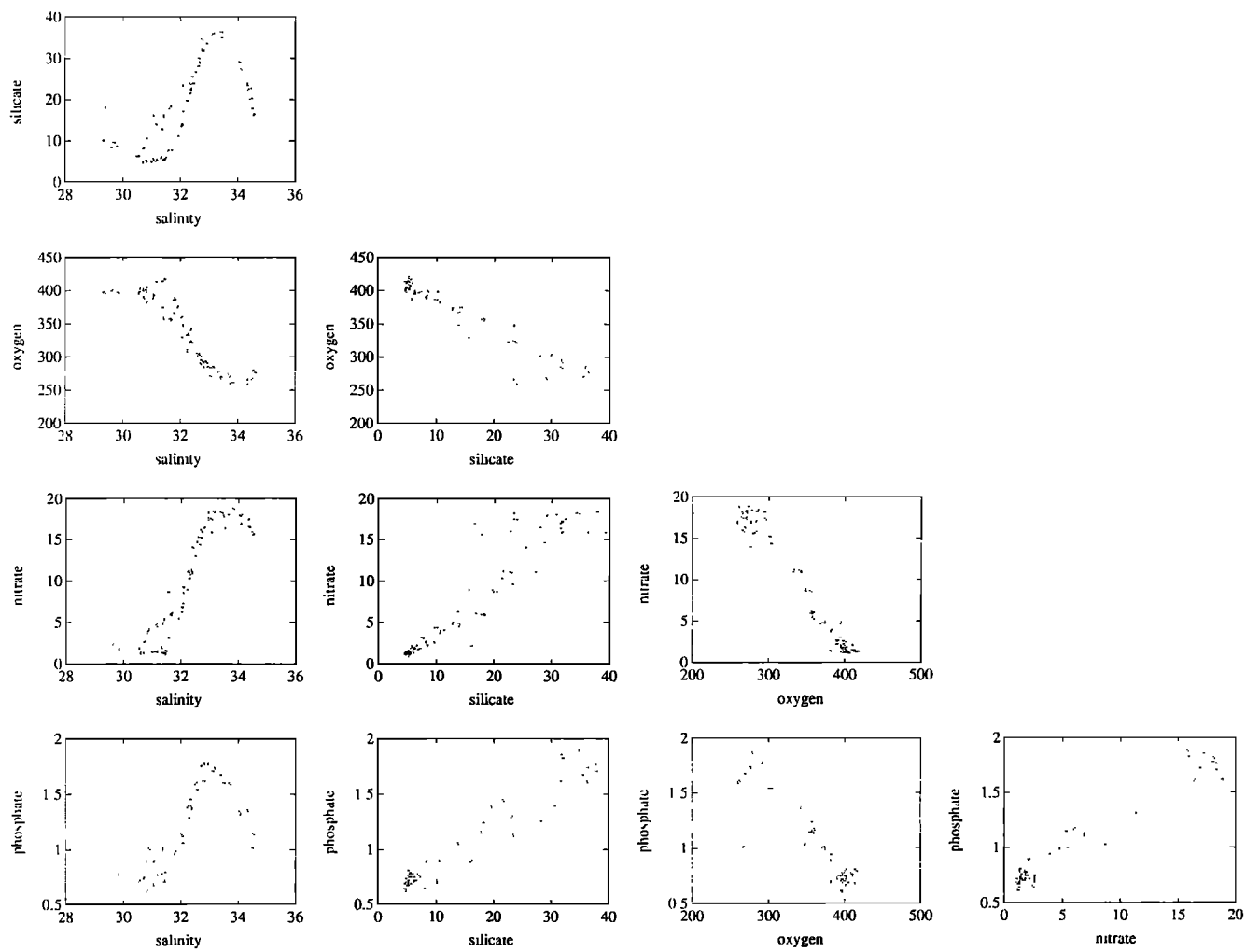

Fig. 2. Scatter plots for the five tracers of the 1987 data set. Nutrient and dissolved oxygen concentrations are in units of micromoles per liter.

by a large local input of fresh water from the Mackenzie in summer and by the large amplitude of the growth-melt cycle in this seasonal sea ice zone. Figure 4 illustrates the range over which near-surface salinity in late winter varied during the 1980s. At the end of the winter of 1980–1981, near-surface salinities were high even far offshore and increased dramatically over the shelf. In March 1989, surface salinities everywhere were below 31 and were fairly uniform

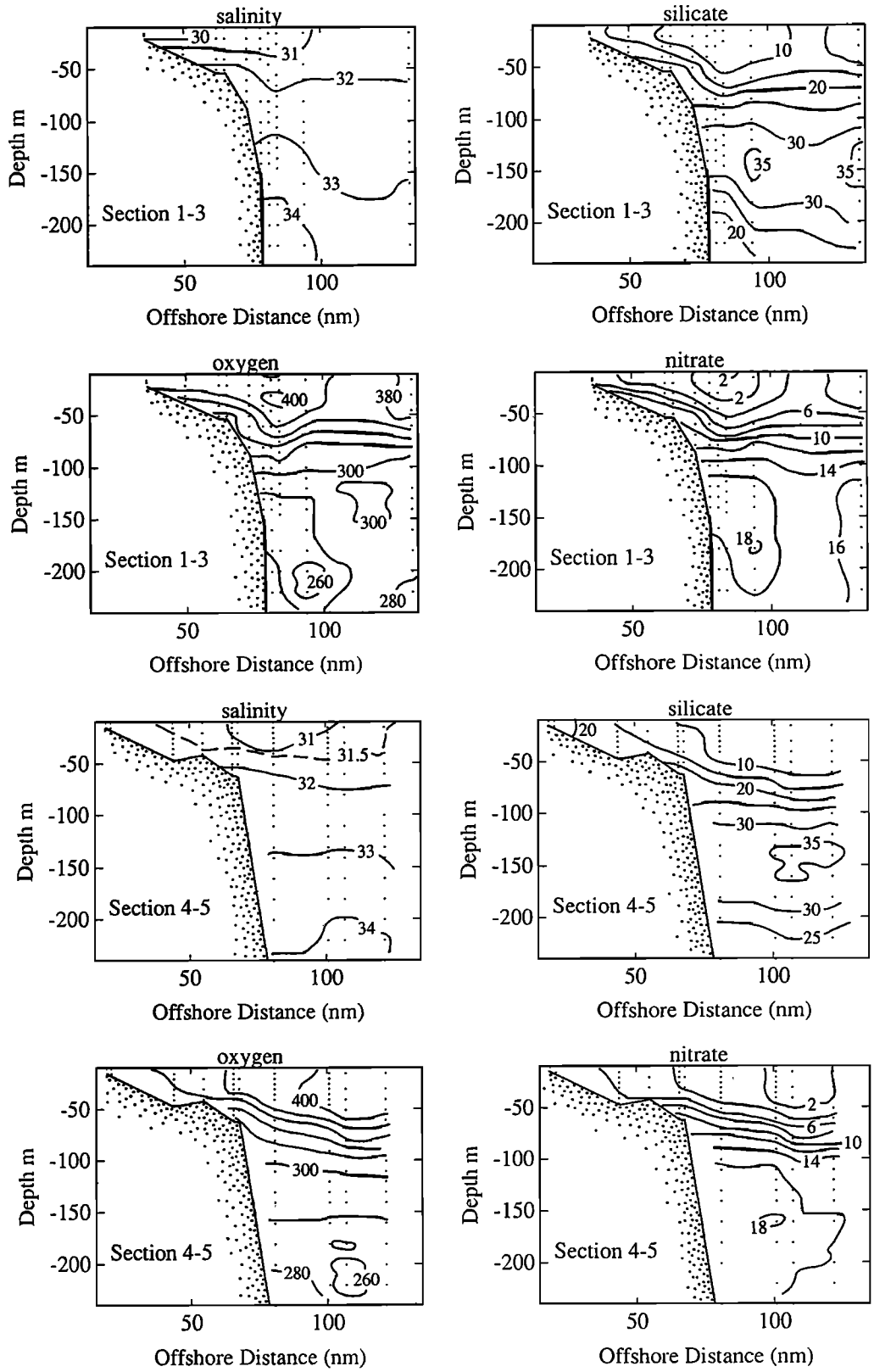

Fig. 3. Salinity, nutrient, and dissolved oxygen sections of 1987 data with three westerly transects grouped together (sections 1–3), and two easterly transects (sections 4 and 5). Nutrient and dissolved oxygen concentrations are in units of micromoles per liter, and distances offshore are in nautical miles (1 n. mi = 1.852 km).

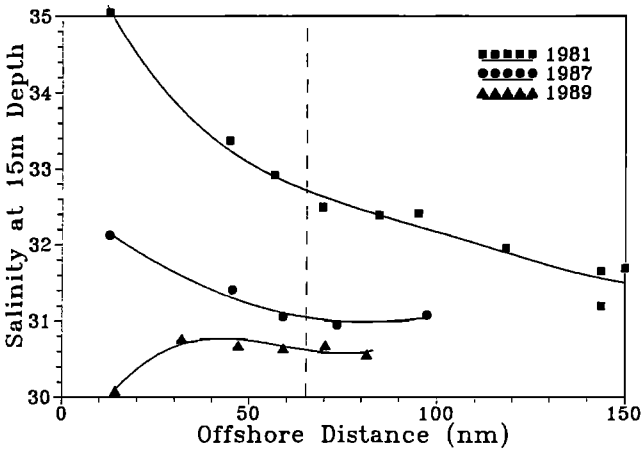

Fig. 4. Salinity at 15 m depth as a function of distance offshore in nautical miles for a line of stations near 130°W. Curves are shown for 1981, when surface salinities were the highest observed for the 1980s; for 1989, when they were the lowest; and for 1987.

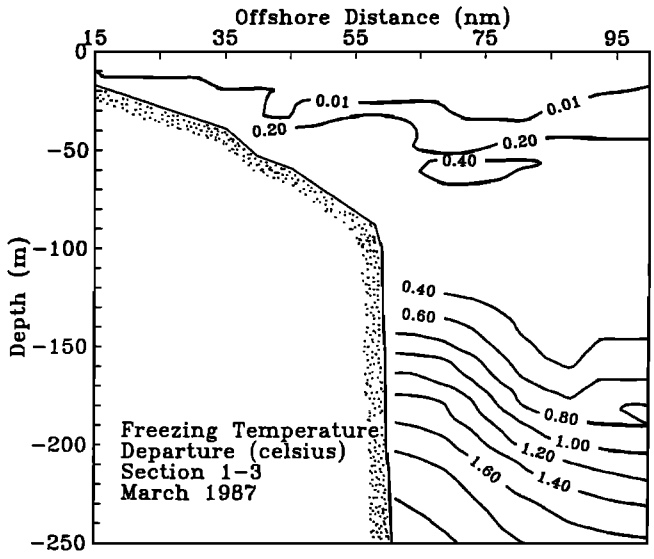

Fig. 5. The departure of water temperatures from freezing point for the three westerly transects in March 1987. Distances offshore are in nautical miles.

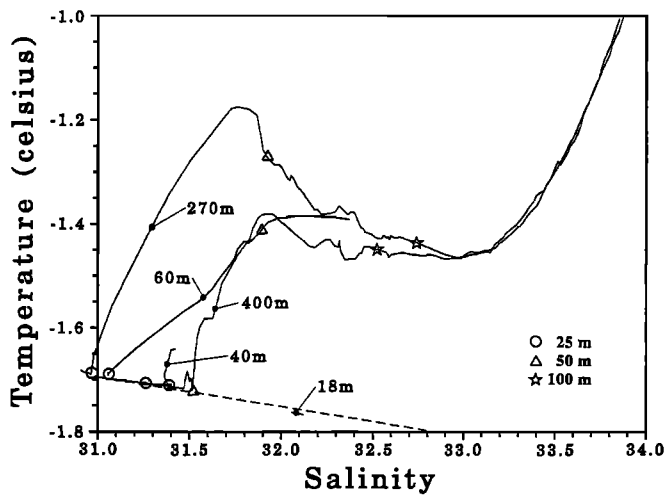

Fig. 6. *T-S* data for the AS section (1987), with the maximum water depth indicated for each profile, and the position of the 25 m, 50 m, and 100 m depths.

over the width of the shelf; at the shallowest station, the effect of freshening by river influence is seen. The data from 1987 which are discussed in this paper are from a winter which falls between oceanographic extremes for this area. Salinities associated with cold waters over the shelf were not sufficiently high to drive ventilation of the halocline in the Canada Basin to the north.

The rejection of brine from growing sea ice plays a major role in the change in surface water salinity between summer and winter [*Melling and Lewis*, 1982]. However, the Mackenzie shelf is the most estuarine of the arctic shelves, with an annual river inflow amounting to about 6 m over its entire area [*Macdonald et al.*, 1987]. Thus because of the large differences between winters, it is unlikely that the growth of ice generates the entire salinity change observed in the area, and it is the extent to which the summertime surface waters of low salinity are exported elsewhere during fall and early winter that is crucial in determining the properties of shelf waters later in the winter. While the inflow of arctic rivers is strongly seasonal, the Mackenzie River is fed by large headwater lakes and has a relatively large wintertime discharge of 10–20% of the summertime peak [*Macdonald et al.*, 1989; *Carmack et al.*, 1989]. It has been observed by *Macdonald and Carmack* [1991] that the heavily ridged ice along the periphery of the landfast ice zone in the Beaufort Sea restricts the spread of river inflow and isolates the offshore zone from its influence in winter. Presumably, the effectiveness of this ice dam varies with ridging conditions from winter to winter.

Variations in the wintertime heat content of shelf waters are associated with differences in wintertime salinities. These variations are an important component of the present climate of the Arctic Ocean because the growth rate and equilibrium thickness of sea ice are very sensitive to small fluxes of heat to the ice from the upper ocean [*Maykut and Untersteiner*, 1971]. In polar oceans, the proximity of the temperature of a water mass to freezing is a reliable indicator of recent exposure of that water mass to the freezing surface interface. Figure 5 is a contoured section of the freezing-temperature departure of waters along sections 1–3 in March 1987. In contrast to conditions in 1981, when shelf waters were at freezing temperature throughout [*Melling*, 1992], there was appreciable heat stored in waters beneath the surface mixed layer in 1987. This heat has its origin in local radiative heating in summer and in advection from warmer seas such as the Bering Sea [*Carmack et al.*, 1989]. One may conclude that during the fall and winter of 1986–1987, the upward transport of heat by entrainment into the overlying turbulent layer, or by upwelling, has been weak. Since temperature and salinity are positively correlated beneath the surface layer, the upward transport of salt by the same mechanisms must also have been weak. This explains, in part, the absence of a water mass of high salinity over the shelf in March 1987.

Temperature-salinity relationships are plotted in Figure 6 for four of the stations on the "AS" line at the eastern end of the shelf. A dashed line on the figure delineates the freezing-temperature relation at atmospheric pressure. Two of the curves, for depths of 40 m and 60 m, illustrate that only the surface water (that of lowest salinity) is at

freezing temperature. However, the remaining curves, for 20 m, 270 m, and 400 m depths, indicate that water at freezing temperature is present below the surface layer; at the shallowest station the full depth range is at the freezing point, and at the deepest station freezing temperatures are maintained to a depth of about 50 m. The low temperature and elevated salinity at the 20 m station indicate the influence of brine addition at this site. These waters could potentially intrude into the layer of elevated temperature at stations further offshore. Since interleaved lenses of freezing temperature, such as reported by *Melling and Lewis* [1982], were not observed over the continental slope in this survey, it is unlikely that any such intrusion has occurred. At the 400 m station, the waters at freezing temperature which intrude under the surface mixed layer are of lower salinity than those at the 20 m station, and only a shallow ventilation to 50 m has occurred. On the portion of this line of observations which overlies the continental shelf, the salinity increases with progression into shallower water. Further west, nearer the delta of the Mackenzie River, this is not the case because surface waters nearshore are freshened by mixing with river inflow.

A second distinctive feature of the water masses of the Mackenzie shelf in wintertime is a pronounced increase below the surface layer in the concentrations of the dissolved nutrients silicate, phosphate, and nitrate (Figure 3), which at the deeper stations reach a local maximum at 130–140 m. Relatively high concentrations of silicate (15–20 μM) are found in shelf waters in wintertime. A decrease in the concentration of dissolved oxygen occurs in conjunction with the increases in dissolved nutrients, although minimum concentrations of dissolved oxygen are attained at a somewhat greater depth of 160 m or more. The 1987 measurements are made to a depth of only 160 m, so the oxygen minimum is not well defined in this data-set. Measurements made to 250 m in 1986 indicate that the oxygen minimum exists in the depth range 180–225 m (salinities 33.8–34.5), with concentrations of around 260 μM. These values may be compared with Canada Basin data compiled by *Wilson and Wallace* [1990] which show oxygen minimum concentrations in the interior of 260–270 μM. Therefore it does not appear that the oxygen minimum near the Mackenzie shelf is any more intense than within the Canada Basin.

A layer of nutrient-rich water centred at a salinity of about 33.1 is found between 100 and 200 m depth throughout much of the western Arctic Ocean [*Kinney et al.*, 1970; *Moore et al.*, 1983]. Its origin has been argued to be inflow through Bering Strait [*Coachman and Barnes*, 1961] or water modified over the continental shelf [*Jones and Anderson*, 1986], or more probably a combination of both [*Moore and Smith*, 1986; *Macdonald et al.*, 1989], with the Chukchi Sea being the probable region for the modification of Bering Strait inflow. It is hypothesized that in the Chukchi Sea the salinity of seawater is increased as a result of a net formation of sea ice and that the concentration of dissolved oxygen is reduced, and that of dissolved nutrients increased, by the oxidation of biogenic material at the sediment-water interface.

Our data show some changes between 1985 and 1987 in the nutrient-salinity relationship of the waters lying on and adjacent to the Mackenzie shelf during winter, as shown in Figure 7. Within the cold halocline (salinity >32.5), silicate concentrations in 1985 were consistently lower than those at the same salinity in 1987. This change over a 2-year period could have been a consequence of an advection of nutrient-rich water into the area by prevailing currents, or of a ventilation of the halocline by nutrient-rich water occurring locally over the same time. Another possibility is that more effective vertical mixing in 1985 lowered the silicate maximum, although this is not supported by any clear concomitant increase in silicate at shallower depths. Neither our observations of temperature, salinity, and dissolved nutrients in the winters of 1985, 1986, and 1987 nor our continuous measurements of current, temperature, and salinity at moorings on the shelf and slope over the same time period indicate that any such ventilation occurred locally. However, an alongshore gradient in the silicate concentration near the nutrient maximum is evident in observations made off the Alaskan north coast. In October 1986, a difference was observed between an average of 29 μM in western Alaskan waters and about 33 μM in the east [*Aagaard et al.*, 1988]. Since the mean current at the depth of the nutrient maximum flows east at about 5 km/d parallel to the shelf edge [*Aagaard*, 1984], a concentration change of the magnitude observed between 1985 and 1987 (Figure 7) could result from advection over a year (although the gradient observed off Alaska late in 1986 would imply that lower concentrations would again prevail in the southeastern Beaufort Sea by 1988). It is quite plausible that temporal variations in the along-shelf gradient in silicate concentration could result from known variations in the flow of water, and silicate, from the Bering Sea [*Aagaard et al.*, 1985*b*].

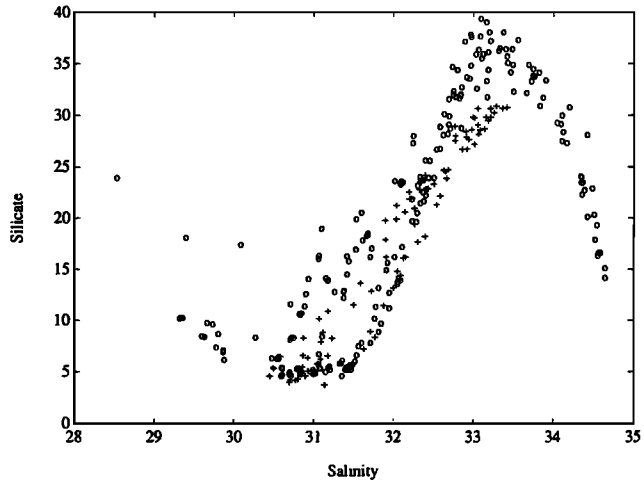

Fig. 7. Silicate-salinity relationship for the years 1985 (crosses) and 1987 (circles). Silicate concentrations are in micromoles per liter.

Oxygen concentrations in the surface waters are generally at or above saturation as a result of the trapping of photosynthetic oxygen by the ice cover and the exclusion of dissolved gas by the accreting ice. For stations in water depths greater than 70 m, the average oxygen supersaturation for waters at or near the surface (upper 15 m) is 3.6%. The shallower stations include some surface undersaturations (average, -1.9%) with the greatest undersaturations, approaching 10%, being at the stations located at the eastern end of the shelf where relatively high salinities have been produced by ice growth. For

example, stations AS0020 and AG0050 have, in the top 15 m, undersaturations of -9.4% and -5.9% respectively. By contrast, the low-salinity shallow stations at the western end of the shelf (e.g., PL0025, PL0030, PL0050) are supersaturated by 3% on average. The undersaturations are interpreted as an effect of salt addition which has driven mixing between surface waters (normally low in silicate) and near-bottom, nutrient-rich, oxygen-depleted waters.

As was mentioned above in connection with the discussion of the nutrient maximum, the oxygen minimum at a salinity of about 34 is thought to result from regenerative processes occurring over shelf sediments, with the Chukchi Sea playing a major role.

INTERACTIONS BETWEEN WATER TYPES IN THE UPPER WATER COLUMN

Scatter plots of all five tracers from the 1987 data set are shown in Figure 2. In this section we present a straightforward statistical method, based on principal component analysis, for reducing this multivariate data set to a more compact form from which end-members may be identified. There are similarities between our approach and those proposed by *Tomczak* [1981] and *Mackas et al.* [1987]. All three approaches assume that a given water sample is a mixture of end-members, and each attempts to determine the mixing ratios from the tracer observations. The main difference between the approach of *Tomczak* [1981] and *Mackas et al.* [1987] is that the latter authors explicitly allow for measurement error and, by using at least as many tracers as end members, reduce the problem of estimating the mixing ratios to one of multiple regression. The main difference between our approach and the other two is that we do not assume that the characteristics of the end-members are known, but rather infer them from the data. Thus although our procedure for reducing observations to a more compact form is objective, our choice of end-members is ultimately subjective. In this sense our approach is closer to an exploratory data analysis technique than that of *Tomczak* [1981] or *Mackas et al.* [1987], both of which are multivariate extensions of classical temperature-salinity diagram techniques for water mass analysis.

Let $\mathbf{x}$ denote the 5×1 vector of observations on a particular water sample. If $\mathbf{x}$ results from the mixing of m end-members, then we may write

$$\mathbf{x} = p_1\mathbf{E}_1 + p_2\mathbf{E}_2 \ldots p_m\mathbf{E}_m + \epsilon \qquad (1)$$

where $\mathbf{E}_i$ is a 5×1 vector defining the characteristics of the ith end-member, p_i is its proportional contribution to the water sample, and ϵ is a residual vector arising from sampling error and processes other than simple mixing. For realizable samples it is clear that the p_i must lie between 0 and 1, and sum to unity. Thus (1) may be rewritten

$$\mathbf{x} = \mathbf{E}_1 + p_2(\mathbf{E}_2 - \mathbf{E}_1) + p_3(\mathbf{E}_3 - \mathbf{E}_1) \ldots p_m(\mathbf{E}_m - \mathbf{E}_1) + \epsilon \qquad (2)$$

Given just two end-members, the observations will lie approximately along the line connecting $\mathbf{E}_1$ and $\mathbf{E}_2$ with scatter due to the residuals. Given three end-members, the observations will lie approximately in the plane connecting $\mathbf{E}_1$, $\mathbf{E}_2$ and $\mathbf{E}_3$. This generalizes in an obvious way to higher dimensions. In this section we describe a method for defining end-members (the $\mathbf{E}_i$) and the associated mixing ratios (the p_i), given a set of oceanographic observations (the $\mathbf{x}$).

Consider first the case of two end-members. The most obvious way to define $\mathbf{E}_1$ and $\mathbf{E}_2$ is to require that the mixing line $\mathbf{E}_2 - \mathbf{E}_1$ pass through the mean of the observations and be aligned with that eigenvector of the 5×5 covariance matrix of observations with the largest eigenvalue ($\mathbf{e}_1$). This approach ensures that the variance of the normal distance of the observation points from the line is a minimum [e.g., *Morrison*, 1978]. This does not of course uniquely determine the two end-members: they can lie anywhere along the mixing line. In practice, the end-members are chosen on the basis of additional information (e.g., the mixing ratios must be nonnegative, salinity must be nonnegative).

For three end-members, it is well known [e.g., *Pearson*, 1901] that the best fitting plane will pass through the mean of the observations ($\overline{\mathbf{x}}$) and will be aligned with those eigenvectors ($\mathbf{e}_1$ and $\mathbf{e}_2$) associated with the two largest eigenvalues. Thus

$$\mathbf{x} = \overline{\mathbf{x}} + z_1\mathbf{e}_1 + z_2\mathbf{e}_2 + \mathbf{e} \qquad (3)$$

where z_1, z_2 are the principal components and $\mathbf{e}$ is a 5×1 error vector which is orthogonal to $\mathbf{e}_1$ and $\mathbf{e}_2$. The plane is "best fitting" in the sense that the sum of $\mathbf{e}'\mathbf{e}$ over all samples is a minimum.

Having defined the plane in terms of $\overline{\mathbf{x}}$, $\mathbf{e}_1$, and $\mathbf{e}_2$, three end-members ($\tilde{\mathbf{E}}_1$, $\tilde{\mathbf{E}}_2$, $\tilde{\mathbf{E}}_3$) that lie on the plane can be chosen. Assuming the end-members are not colinear, then in accord with (1) we may write

$$x = p_1\tilde{\mathbf{E}}_1 + p_2\tilde{\mathbf{E}}_2 + p_3\tilde{\mathbf{E}}_3 + \mathbf{e} \qquad (4)$$

where the p_i are the mixing ratios, readily obtained from z_1 and z_2, and $\mathbf{e}$ is the same as in (3). The extension of this approach to more eigenvectors, and hence more end-members is straightforward.

Note that since the plane of best fit depends on the units of the observations, we decided to scale the data prior to analysis. We first scaled observations of the same type by their standard deviation. This is equivalent to replacing the covariance matrix by the correlation matrix. We then tried scaling the observations by their analytical errors. We found that the end-members were similar for both schemes, after they had been rescaled.

In practice it may not be obvious a priori how many eigenvectors are required to describe the data. From an oceanographic point of view, the addition of extra eigenvectors should cease when the variance of the errors in (4) is lower than that expected from the combined effect of analytical error, measurement error, and model misspecification. From a statistical perspective the addition of extra eigenvectors should cease when they fail to account for a statistically significant proportion of the variance. *Preisendorfer* [1988] describes several methods for determining the number of significant eigenvalues and hence the number of end-members.

We will now describe a principal component analysis of the data collected in 1987 in the upper 120 m of the water column. In all that follows, observations of the same type were scaled by their standard deviation prior to analysis. The proportion of total variance explained

TABLE 1. Statistics of Measured Parameters and Results of Principal Component Analysis

	S	Si	O_2	N	P
Standard deviation	0.93	9.27 μM	41.78 μM	5.27 μM	0.37 μM
Proportion of variance accounted for by e_1 and e_2	0.998	0.975	0.956	0.982	0.958
Standard deviation of variability unaccounted for by e_1 and e_2.	0.04	1.47 μM	8.80 μM	0.70 μM	0.80 μM
Estimated analytical errors (1σ)	0.005	0.15 μM	1μM	0.1 μM	0.04 μM

by just two eigenvectors is 97.4%. A calculation has also been made of the standard deviation of the errors that result from assuming that two eigenvectors, and hence three end-members, are sufficient to describe the distribution of these water properties. In particular, for each sample we calculated the difference between observed S, Si, O_2, NO_3, and P and the model representation of these properties based on two eigenvectors. The standard deviations of these differences are given by the third row of numbers in Table 1. As was mentioned above, these errors include measurement errors as well as deficiencies in the model. The standard deviations of our five tracers, and that proportion of the variance which can be accounted for by e_1 and e_2, are also given in Table 1. Clearly, salinity is particularly well described by the first two eigenvectors, even though the five tracers were standardized to unit variance before analysis. For comparison we have also listed the estimated analytical errors. They are generally much smaller than the errors arising from our description based on two eigenvectors. However, given that we aim to provide a simple description as possible of the system and that the analytical errors do not include sampling error, we will henceforth describe the observations using just two eigenvectors.

Figure 8 is a scatter plot of z_2 against z_1. To exemplify how the concentrations of tracers vary across the plane, we have superimposed on this plot contours of salinity and silicate. It is clear from this figure that three end-members

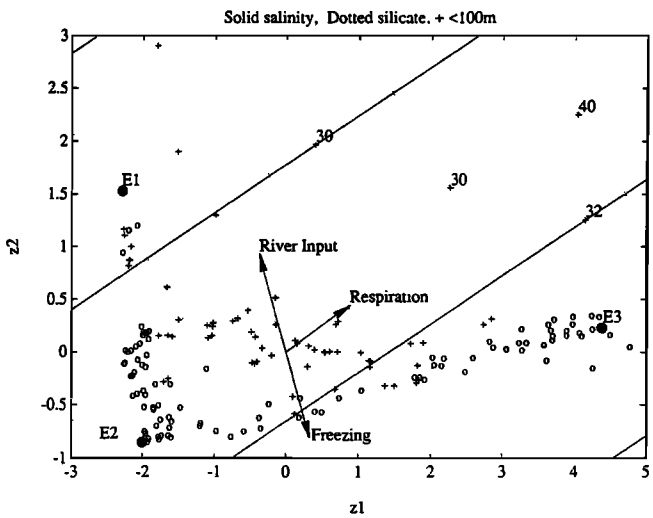

Fig. 8. Plot of z_2 versus z_1 for the 1987 samples from depths <120 m. For stations in water depth greater than 100 m, data points are denoted by circles, and for shallower stations, by crosses. Contours of salinity (solid lines) and silicate (dotted lines) are superimposed. Positions of end-members E1, E2, and E3 are shown. The arrows indicate the effects of river runoff, respiration, and freezing.

may be identified; these are denoted by E1, E2, and E3. Notice that the majority of the points fall within the triangle formed by the selected end-members; this ensures that the majority of mixing ratios will lie between 0 and 1. (If the end-members were selected so that they would encompass all the data points, undue weight would be given to a small number of outlying samples.) In this figure the data are separated into two groups, the stations in water depth greater than 100 m, denoted by circles, and those shallower, denoted by crosses; this approximates the stations on the shelf and those beyond the shelf break. In the diagram these two groups are for the most part quite distinct, the end-member E2 naturally becoming increasingly prominent in the more offshore, deeper stations, but the stations with water depths less than 100 m are still clearly influenced by this offshore component.

From the coordinates of the selected end-members on the z_1, z_2 plane their properties have been recalculated, and the values are given in Table 2 in the original units.

The end-members E1, E2, and E3 represent water from shallow inshore stations (influenced by river inflow), waters of the surface mixed layer (from the stations furthest offshore, most closely matched by properties at station AS1000 (Figure 1)), and the nutrient maximum layer, respectively. Their interactions as indicated by Figure 8 involve horizontal mixing across the shelf between the inshore and offshore surface waters and vertical mixing offshore between nutrient maximum water and surface water. The nutrient maximum water itself lies too deep to occur in pure form on the shelf, but over the shelf there is mixing between the surface layer and bottom waters that have properties intermediate between the nutrient maximum water and offshore surface waters. Mixing between the end-members E2 and E3 apparently occurs predominantly by diapycnal processes over the outer continental shelf and upper continental slope. *Melling et al.* [1984] discuss diapycnal mixing in the waters below 250 m in this zone and estimate that the diapycnal diffusivity at these depths is quite small. An effective mixing process is the entrainment of E3 waters into the surface mixed layer which is predominantly of E2 composition in this area. This entrainment is countered by an upwelling of E3 water so that a stable mixed layer depth is maintained. *Melling* [1992] estimates that this entrainment, which is driven primarily

TABLE 2. Properties of End-Members Selected From Figure 8

End-Member	S	Si, μM	O_2, μM	N, μM	P, μM
E1: inshore surface	29.32	10.9	399	2.1	0.71
E2: offshore surface	31.40	3.3	410	0.7	0.71
E3: nutrient maximum	32.92	34.1	280	17.3	1.82

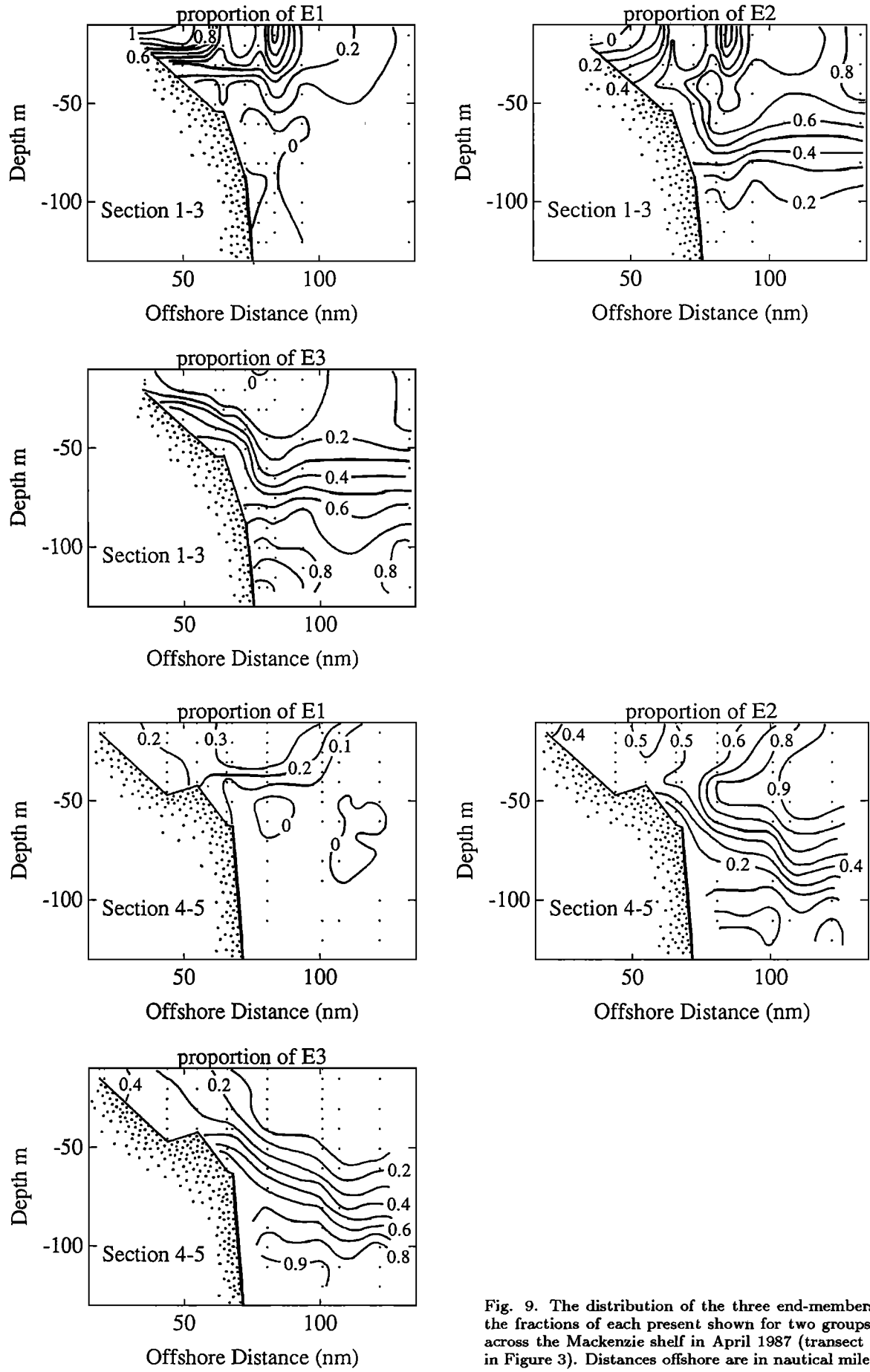

Fig. 9. The distribution of the three end-members in terms of the fractions of each present shown for two groups of transects across the Mackenzie shelf in April 1987 (transect groupings as in Figure 3). Distances offshore are in nautical miles.

by convectively driven turbulence, proceeds at a rate of 10–20 cm/d. Over a period of months, E3 waters entrained at this rate can constitute perhaps 20% of the mixed layer over the outer shelf.

The proportions of each of these end-members that are required to yield the properties of the rest of the points have been calculated. Each water sample is now approximated by the three mixing ratios: p_1, p_2, and p_3 as defined in equation (4). Using the same transects and groupings of stations as in Figure 3, we have plotted the mixing ratios across the shelf (Figure 9).

The low-salinity inshore end-member (E1) is seen to be much more pronounced in the westerly group of sections (1–3) which are more influenced by the Mackenzie River. The figure suggests that the end-member having the properties of offshore surface water (E2) intrudes into the water column lying over the continental shelf. Such an intrusion would be consistent with an offshore flow of either or both surface and bottom waters. The first of these could be driven by the supply of a low-salinity surface layer from river runoff, and the second, by salt addition to shallow waters. Both groups of sections show the intrusion of the nutrient maximum component up onto the shelf. The occurrence of this water on the shelf in winter at locations having water depths as shallow as 50 m represents a major difference from the situation in summer. *Carmack et al.* [1989] report that the highest salinity water crossing the shelf break onto the shelf is 32.3, and even this is limited to the outer half of the shelf where water depths exceed 50 m.

It is of interest to compare end-members selected herein by the principal components method with those selected by *Macdonald et al.* [1989] in the interpretation of observations made in the same area 6 months earlier. *Macdonald et al.* [1989] use five end-members, of which two (their "PML" and their "33.1") correspond to the E2 and E3 discussed here. Table 3 presents the comparison.

The 33.1 water type is higher in dissolved silicate than the E3 end-member. This is in part due to our selected cutoff depth of 120 m, when somewhat higher levels ($\sim$ 37 μM) occur at some deeper stations at around 140–160 m. However, if we include all waters to these greater depths, the result is that an additional end-member is required to describe observations at locations where the silicate maximum is relatively shallow. Our wintertime data sets do not show waters having silicate concentrations as high as 45 μM. This may explain why *Macdonald et al.* [1989] have to mix a significant percentage (30%) of other water types (with lower nutrient concentrations) to the 33.1 water type to obtain the observed water of 33.1 salinity. It is evident that the particular selection of properties for mixing end-members has a significant effect on the calculated mixing fractions.

Amongst the most important processes affecting chemical and physical properties are freezing of seawater, melting of sea ice, photosynthesis and respiration, and the addition of fresh water from the Mackenzie River. We will now examine the way in which each of these processes moves the properties of a water parcel around the z_1–z_2 plane which has been defined for the 1987 data set.

First consider a unit change in salinity due to freezing: all the other dissolved constituents are assumed to increase in the same proportion as salinity. Similarly, we consider a unit decrease in salinity due to the addition of Mackenzie River water. The properties of this water (S, Si, N, P) are taken from *Macdonald et al.* [1989], and in the absence of knowledge of the dissolved oxygen content, it is assumed to be saturated relative to the atmosphere at a temperature of 0°C.

An increase in phosphate of 0.5 μmol due to respiration was arbitrarily selected with changes in the other properties being set by the ratio, P:N:O:Si, 1:16:172:50 [*Takahashi et al.*, 1985; *Broecker and Peng*, 1982], salinity being unaffected. Photosynthesis would give the opposite changes (i.e., a reduction in each of the nutrient concentrations).

Thus for each of the above processes we can define a change in our five tracers which we will denote by Δx. In accord with our scaling procedure, each element of Δx was divided by the standard deviation of the corresponding tracer. To standardize the length of the scaled Δx, we then normalized its length to unity. The result is that for each of the processes we have defined a unit vector in the five-dimensional space of standardized tracers. If a process causes changes only within the plane, the projection of the unit vector will have length equal to 1, while if the process operates perpendicular to the plane the projection length will be zero. The projections of the vectors onto the z_1–z_2 plane are shown in Figure 8, where they radiate from a point that represents the average properties of all the samples. It is found that addition of river water lies closest to the plane with a projection of length 0.995; respiration/photosynthesis also operates almost entirely within the plane, the projection length being 0.984. The effect of freezing/melting is less confined to the plane, although the projection length is still high at 0.934.

Since any two of these processes must define a plane of water properties, it is significant that the plane which we find to describe all the water properties in the top 120 m is almost identical with that resulting from photosynthesis/respiration and the supply of river water. The observation that the salt addition, caused by sea ice production, moves points out of the plane suggests that according to the quantity of sea ice that is produced from year to year, the position of the plane in space might vary, or some water bodies (probably those from shallow locations where the influence of salt addition should be greatest) might be moved off the plane, yielding a curved surface.

TABLE 3. Comparison of End-Members Selected by the Principal Components Method With Those Selected by *Macdonald et al.* [1989]

Water Type	Salinity	Silicate, μM	Nitrate, μM	Phosphate, μM
E2 (offshore surface)	31.4	3.3	0.7	0.71
PML (winter surface)	31.6	4.7	1.0	0.80
E3 (nutrient maximum)	32.9	34.1	17.3	1.82
33.1 (upper halocline)	33.1	45.0	20.0	2.30

If the entire data set for 1987 is analyzed, the additional points corresponding to samples below 120 m appear on the z_1, z_2 plot as an arm extending from E3. It is therefore clear that an additional end-member is required to describe variations beneath the nutrient maximum. With a four-component system it would not normally be expected that all the tracer properties would lie in a two-dimensional plane as required for a three-component system. However, the variance accounted for by the first two principal components is still high: 97.1%.

A probable explanation for why the additional end-member comes close to lying in the same plane is that this water has also acquired its own distinct properties by the same processes that have been referred to above. These processes we find are constrained to alter our set of tracers within space that tends toward two dimensions. Additional or alternative tracers that are independent of freshwater dilution and biological processes should avoid this shortcoming.

CONCLUSIONS

Wintertime salinities on the Beaufort Sea shelf are always markedly higher than the summertime values, but year to year variability is high, and it is not commonly observed that densities can reach levels sufficiently high for the shelf waters to provide a source of intermediate or deep waters to the Arctic Ocean. Conditioning of the system in the fall or early winter, in such a way as to reduce the amount of river-derived fresh water, is believed to be one of the main processes which permits this region occasionally to yield high-salinity waters during the winter.

For a data set collected in late winter of 1987 and for depths down to about 120 m, salinity, nutrients, and oxygen can be modelled as the products of mixing between an inshore surface component, an offshore surface mixed-layer component, and water from the nutrient maximum layer. In the case of these upper waters, at least in the late winter of 1987, it appears that the interacting water masses have their different chemical properties maintained mainly by river runoff and by photosynthesis and nutrient regeneration.

While the mixing model based on the end-members selected by the principal components method does a respectable job of representing the chemical properties of arctic surface and halocline waters, it does poorly with temperature. Waters whose salinities are typical of the three end-members E1, E2, and E3 have temperatures of -1.6°, -1.72°, and -1.46°C, respectively. Thus no water with a temperature higher than -1.46°C can be generated by mixing of the end-members. However, it is evident from Figure 6 that a significant volume of water warmer than this is present.

The apparent paradox can be resolved if it is acknowledged that the mixing of end-members is complemented by other processes in shaping the hydrography of the area. Near-surface waters may warm and cool with the passage of the seasons without change in their chemical characteristics. It is already recognized that seasonal processes will alter the nutrient concentrations due to biological activity, so that the mixing model is only applicable over such time scales as the nutrients behave almost conservatively. It may be concluded that temperature is varying within this system on a shorter time scale than biological processes, which is not surprising for the winter season.

The observation that salt addition, caused by sea ice production, moves points out of the plane suggests that according to the quantity of sea ice that is produced from year to year, the position of the plane in space might vary, or some water bodies (probably those from shallow locations where the influence of salt addition should be greatest) might be moved off the plane.

A fourth component is required to account for the properties of waters down to 250 m. The fact that the additional component, while not lying in the same plane as the first three, remains close to that plane suggests that this water body which lies below the nutrient maximum has been produced by similar processes.

This analysis demonstrates that principal component analysis will be most effective in revealing end-members when the tracers used are quite independent in the sense that they are being operated upon by fundamentally different processes. Thus while several waters may have quite distinct nutrient and oxygen concentrations, and so have clearly defined end-member characteristics, they may lie in or close to a plane on account of the small number of processes that originally produced most of the property variation, by acting on the different components in related ways. Prime examples of such processes are respiration/photosynthesis, and dilution with freshwater or evaporation. It is implicit in the treatment described above that a further limitation on the use of a simple mixing model lies in the seasonally changing properties of the waters, e.g., the freshening of the surface layer in spring with ice melt and increase in runoff. This results in time-varying properties of the end-members and means that properties need not plot as simple linear mixtures.

Acknowledgments. This work was supported by the Natural Sciences and Engineering Research Council of Canada, by the Department of Fisheries and Oceans Canada, by the Federal Panel on Energy Research and Development, and by the Polar Continental Shelf Project. The able assistance of S. W. Moorhouse, R. A. Cooke, S. Niven, R. Pett, and X. Zhou during preparations and field work is gratefully acknowledged. During the preparation of the final manuscript, the comments of an anonymous reviewer and the assistance of J. Hurst were most valuable.

REFERENCES

Aagaard, K., The Beaufort Sea undercurrent, in: *The Alaskan Beaufort Sea, Ecosystems and Environments*, edited by P.W. Barnes, D.M. Schell, and E. Reimnitz, pp. 47–71, Academic, San Diego, Calif., 1984.

Aagaard, K., A synthesis of the Arctic Ocean circulation. *Rapp. P. V. Reun. Cons. Int. Explor. Mer, 188*, 11–22, 1989.

Aagaard, K., L.K. Coachman, and E.C. Carmack, On the halocline of the Arctic Ocean, *Deep Sea Res., Part A, 28*, 529–545, 1981.

Aagaard, K., A.T. Roach, and J.D. Schumacher, On the wind-driven variability of the flow through Bering Strait, *J. Geophys. Res., 90*, 7213–7221, 1985*a*.

Aagaard, K., J.H. Swift, and E.C. Carmack, Thermohaline circulation in the Arctic mediterranean seas, *J. Geophys. Res., 90*, 4833–4846, 1985*b*.

Aagaard, K., S.A. Salo, and K. Krogslund, Beaufort Mesoscale Circulation Study: Hydrography USCGC *Polar Star* cruise, October 1986, *NOAA Tech. Memo. ERL PMEL-19*, 83 pp., Pac. Mar. Environ. Lab., Seattle, Wash., 1988.

Broecker, W.S., and T-H. Peng, *Tracers in the Sea*, Lamont-Doherty Geological Observatory, Columbia University, Palisades, N.Y., 1982.

Carmack, E.C., R.W. Macdonald, and J.E. Papadakis, Water

mass structure and boundaries in the Mackenzie shelf estuary, *J. Geophys. Res., 94*, 18,043–18,055, 1989.

Coachman, L.K., and C.A. Barnes, The contribution of Bering Sea water to the Arctic Ocean, *Arctic, 14*, 147–161, 1961.

Jones, E.P., and L.G. Anderson, On the origin of the chemical properties of the Arctic Ocean halocline, *J. Geophys. Res., 91*, 10,759–10,767, 1986.

Kinney, P., M.E. Arhelger, and D.C. Burrell, Chemical characteristics of water masses in the Amerasian Basin of the Arctic Ocean, *J. Geophys. Res., 75*, 4097–4014, 1970.

Macdonald, R.W., and E.C. Carmack, The role of under-ice topography in separating estuary and ocean on an arctic shelf, *Atmosphere-Ocean, 29*(1), 37–53, 1991.

Macdonald, R.W., C.S. Wong, and P.E. Erickson, The distribution of nutrients in the southeastern Beaufort Sea: Implications for water circulation and primary production, *J. Geophys. Res., 92*, 2939–2952, 1987.

Macdonald, R.W., E.C. Carmack, F.A. McLaughlin, K. Iseki, D.M. Macdonald, and M.C. O'Brien, Composition and modification of water masses in the Mackenzie shelf estuary, *J. Geophys. Res., 94*, 18,057–18,070, 1989.

Mackas, D.L., K.L. Denman, and A.F. Bennett, Least squares multiple tracer analysis of water mass composition, *J. Geophys. Res., 92*, 2907–2918, 1987.

Maykut, G.A., and N. Untersteiner, Some results from a time-dependent thermodynamic model of sea ice, *J. Geophys. Res., 76*, 1550–1575, 1971.

Melling H., The formation of a haline shelf front in wintertime in an ice-covered arctic sea, *Cont. Shelf Res.*, in press, 1992.

Melling, H., and E.L. Lewis, Shelf drainage flows in the Beaufort Sea and their effect on the Arctic Ocean pycnocline, *Deep Sea Res., 29*, 967–985, 1982.

Melling, H., R. A. Lake, D. R. Topham, and D.B. Fissel, Oceanic thermal structure in the western Canadian Arctic, *Cont. Shelf Res., 3*, 233–258, 1984.

Midttun, L., Formation of dense bottom water in the Barents Sea, *Deep Sea Res., 32*, 1233–1241, 1985.

Moore, R.M., and J.N. Smith, Disequilibria between Ra-226, Pb-210 and Po-210 in the Arctic Ocean and the implications for chemical modification of the Pacific water inflow, *Earth Planet. Sci. Lett., 77*, 285–292, 1986.

Moore, R.M., M.G. Lowings, and F. Tan, Geochemical profiles in the central Arctic Ocean: Their relationship to freezing and shallow circulation, *J. Geophys. Res., 88*, 2667–2674, 1983.

Morrison, D.F., *Multivariate Statistical Methods*, 415 pp., McGraw-Hill, New York, 1978.

Nansen, F., Northern waters: Captain Roald Amundsen's oceanographic observations in the Arctic seas in 1901, *Videnskabs selsk. Skr. Kl., I Mat. - Naturvidensk. Kla., 3*, 145 pp., 1906.

Pearson, K., On lines and planes of closest fit to systems of points in space, *Philos. Mag., 6*(2), 559–572, 1901.

Preisendorfer, R.W., *Principal Component Analysis in Meteorology and Oceanography, Develop. Atmos. Sci.*, vol. 17, 425 pp., Elsevier, New York, 1988.

Strickland, J.D.M., and T.R. Parsons, A practical handbook of seawater analysis, *Bull. Fish. Res. Board Can., 167*, 310 pp., 1972.

Takahashi, T., W.S. Broecker, and S. Langer, Redfield ratio based on chemical data from isopycnal surfaces, *J. Geophys. Res., 90*, 6907–6924, 1985.

Tomczak, M., A multi-parameter extension of temperature/salinity diagram techniques for the analysis of nonisopycnal mixing, *Prog. Oceanogr., 10*, 147–171, 1981.

Wilson, C., and D.W.R. Wallace, Using the nutrient NO/PO as a tracer of continental shelf waters in the central Arctic Ocean, *J. Geophys. Res., 95*, 22,193–22,208, 1990.

H. Melling, Institute of Ocean Sciences, Sidney, British Columbia, Canada V8L 4B2

R. M. Moore and K. R. Thompson, Department of Oceanography, Dalhousie University, Halifax, Nova Scotia, Canada B3H 4J1

(Received August 5, 1991;
revised January 16, 1992;
accepted March 1, 1992.)